Molecular Therapy
Original Article

Tubular-specific CDK12 knockout causes a defect in urine concentration due to premature cleavage of the *slc12a1* gene

Bin Wang,[1,4] Yao Wang,[2,3,4] Yi Wen,[1] Yi-Lin Zhang,[1] Wei-Jie Ni,[1] Tao-Tao Tang,[1] Jing-Yuan Cao,[1] Qing Yin,[1] Wei Jiang,[1] Di Yin,[1] Zuo-Lin Li,[1] Lin-Li Lv,[1] and Bi-Cheng Liu[1,2]

[1]Institute of Nephrology, Zhong da Hospital, Southeast University School of Medicine, No. 87, Dingjiaqiao Road, Gulou District, Nanjing, Jiangsu Province, China; [2]Nanjing Medical University, Nanjing, Jiangsu, China; [3]Department of Nephrology, The Affiliated Hospital of Yangzhou University, Yangzhou University, Yangzhou, Jiangsu, China

Cyclin-dependent kinase 12 (CDK12) plays a critical role in regulating gene transcription. CDK12 inhibition is a potential anticancer therapeutic strategy. However, several clinical trials have shown that CDK inhibitors might cause renal dysfunction and electrolyte disorders. CDK12 is abundant in renal tubular epithelial cells (RTECs), but the exact role of CDK12 in renal physiology remains unclear. Genetic knockout of CDK12 in mouse RTECs causes polydipsia, polyuria, and hydronephrosis. This phenotype is caused by defects in water reabsorption that are the result of reduced Na-K-2Cl cotransporter 2 (NKCC2) levels in the kidney. In addition, CKD12 knockout causes an increase in *Slc12a1* (which encodes NKCC2) intronic polyadenylation events, which results in *Slc12a1* truncated transcript production and NKCC2 downregulation. These findings provide novel insight into CDK12 being necessary for maintaining renal homeostasis by regulating NKCC2 transcription, which explains the critical water and electrolyte disturbance that occurs during the application of CDK12 inhibitors for cancer treatment. Therefore, there are safety concerns about the clinical use of these new anticancer drugs.

INTRODUCTION

Cyclin-dependent kinase 12 (CDK12), first isolated and characterized by Ko et al. in 2001, belongs to the transcription-related cyclin-dependent kinase (CDK) family.[1] CDK12 maps on chromosome 17q12, which contains oncogene and genetic alterations in various tumors.[2] Next-generation sequencing data suggested that CDK12 mutation is common in cancers.[3,4] CDK12 depletion attenuates DNA damage response (DDR) gene expression and promotes tumorigenesis.[5] In preclinical studies, CDK12 depletion resulted in synthetic lethality in response to poly (ADP-ribose) polymerase (PARP) inhibitors (olaparib) and increased cisplatin and olaparib cytotoxicity.[6]

By targeting CDK12 and CDK13, the covalent inhibitor THZ531 exhibits potent efficacy in a variety of cancers.[7–9] Dinaciclib, a pan-CDK inhibitor, potently inhibits CDK12 activity (half-maximal inhibitory concentration [IC50] = 0.050 μM) and is commonly used in clinical trials.[10] There are 18 registered dinaciclib studies in the clinicaltrials.gov global database, using dinaciclib only or in combination with chemotherapeutic compounds. Among these dinaciclib studies, 6 clinical trials reported that dinaciclib causes renal adverse effects, including hyperuricemia, creatinine elevation, hypokalemia, hyponatremia, and hypotension (Date base: https://clinicaltrials.gov). Furthermore, a genome-wide association and functional follow-up with 130,600 European ancestry participants demonstrated that *CDK12* loci are negatively associated with the estimated glomerular filtration rate (eGFR).[11] In the kidney, CDK12 is abundantly expressed in renal tubular epithelial cells (https://www.proteinatlas.org).

CDK12 deficiency results in embryonic lethality shortly after implantation, as increased apoptosis in CDK12$^{-/-}$ blastocysts prevents the outgrowth of the inner cell mass.[12] To clarify the role of CDK12 in renal physiology and metabolism, we generated a conditional mutant mouse line that harbors CDK12 deletion selectively in renal tubular epithelial cells (RTECs). Interestingly, the RTEC-specific CDK12 knockout mice presented with striking urine concentration defects, which may explain the renal side effects of CDK12 inhibition in clinical trials of malignancy. Our study highlighted a novel role of CDK12 in regulating salt and water homeostasis in the kidney, which suggested particular safety concerns about renal side effects during the application of CDK12 inhibitors as anticancer agents.

RESULTS

Generation of mice with specific deletion of CDK12 in RTECs

To explore the function of CDK12 in the kidney, we generated a novel *CDK12*$^{flox/flox}$ line harboring loxP sites flanking exon 4 of the *Cdk12* gene. By breeding with cdh16-Cre transgene mice, in which Cre

Received 3 December 2021; accepted 11 May 2022;
https://doi.org/10.1016/j.ymthe.2022.05.012.

[4]These authors contributed equally

Correspondence: Yi Wen, MD, PhD, Institute of Nephrology, Zhongda Hospital, Southeast University School of Medicine, No. 87, Dingjiaqiao Road, Gulou District, Nanjing, Jiangsu Province, China.
E-mail: wy3511362@126.com
Correspondence: Bi-Cheng Liu, MD, PhD, Institute of Nephrology, Zhongda Hospital, Southeast University School of Medicine, No. 87, Dingjiaqiao Road, Gulou District, Nanjing, Jiangsu Province, China.
E-mail: liubc64@163.com

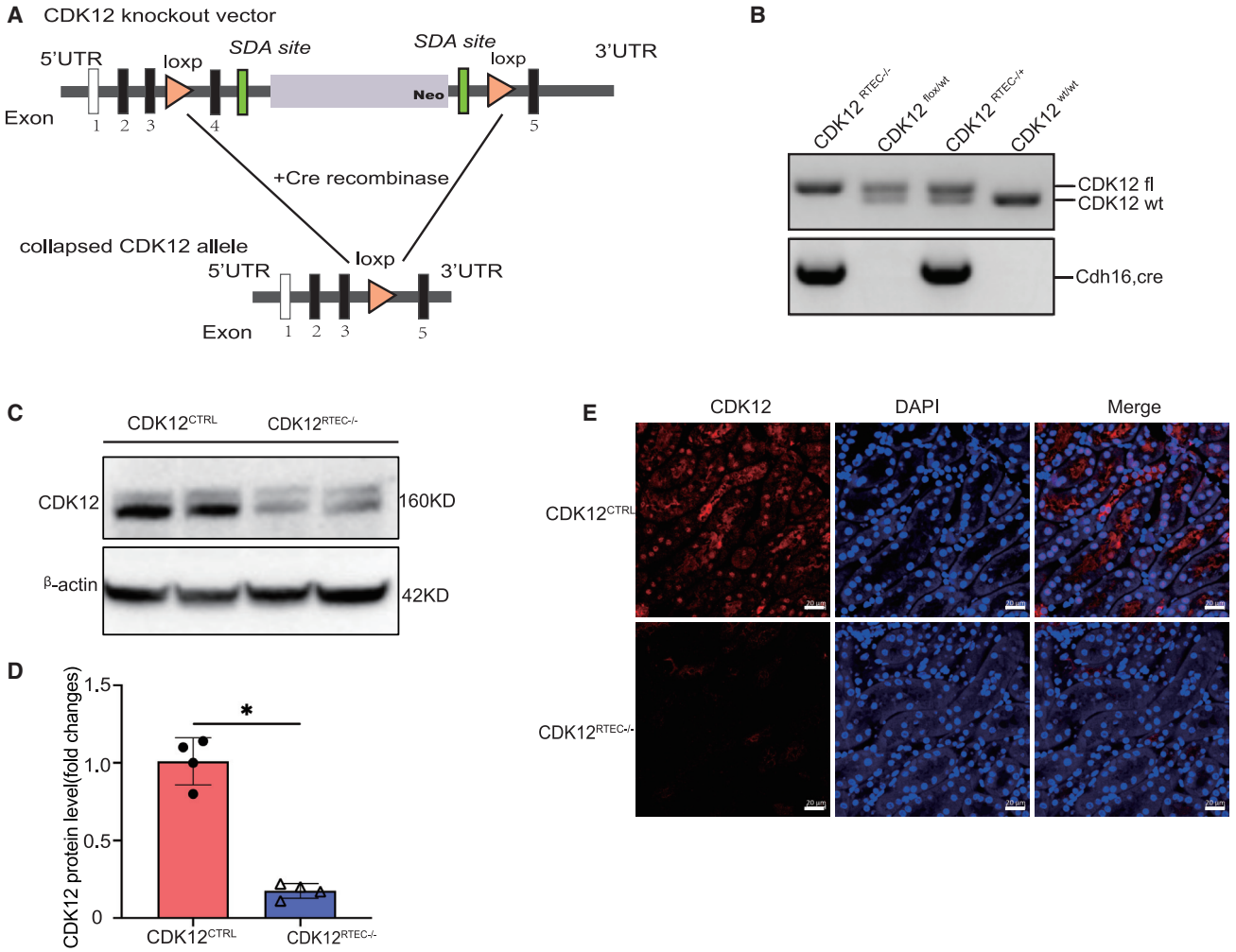

Figure 1. Production and verification of the CDK12 renal tubular cell knockout mouse model

(A) Schematic of the CKD12-ko vector showing *loxp* sites flanking exon 4, the gene encoding CDK12 (3.1% of the coding region). (B) Representative images of CDK12 *flox* and *Cdh16-Cre* determination. (C and D) Western blot analysis of CDK12 in kidney tissues. Data are presented as the means ± SE, n = 4. (E) Representative confocal images show the changes in CDK12 in the nuclei of tubules in paraffin-embedded kidney sections. Scale bars, 20 μm. *p < 0.05 versus $CDK12^{CTRL}$ group, unpaired t-test.

expression is limited to the renal tubules, including Bowman's capsule, proximal tubule, loop of Henle, distal tubule, and the collecting duct, we produced *cdh16-Cre*$^{+}$ *CDK12*$^{flox/flox}$ mice ($CDK12^{RTEC-/-}$) and *cdh16-Cre*$^{-}$ *CDK12*$^{flox/flox}$ littermates ($CKD12^{CTRL}$) (Figure 1A).[13] $CDK12^{RTEC-/-}$ and $CDK12^{CTRL}$ mice were genotyped using a PCR method (Figure 1B). Consistently, $CDK12^{RTEC-/-}$ mice exhibited CDK12 protein deficiency compared with $CDK12^{CTRL}$ mice (Figures 1C and 1D). Using immunofluorescence staining, we found that CDK12 protein was mainly expressed in the nucleus of RTECs and was blocked by RTEC-specific CDK12 deletion (Figure 1E).

RTEC-specific CDK12 deletion leads to polyuria with low osmolality of the urine

There was no difference in gross appearance between $CDK12^{RTEC-/-}$ and $CDK12^{CTRL}$ mice. Interestingly, $CDK12^{RTEC-/-}$ mice exhibited severe polyuria and polydipsia, as evidenced by excessive urination and thirst. After being placed in metabolic cages overnight, $CDK12^{RTEC-/-}$ mice exhibited a 5-fold higher urine volume and lower osmolality than $CDK12^{CTRL}$ mice (Figures 2A–2C). As shown in Figure 2D, water consumption by $CDK12^{RTEC-/-}$ mice was 5-fold higher than that of $CDK12^{CTRL}$ mice. The body weights were similar between the $CDK12^{RTEC-/-}$ and $CDK12^{CTRL}$ groups (Figure 2E). These data suggested that RETC-specific deletion of CDK12 induced excessive thirst and diluted urine excretion, possibly due to a renal concentration defect.

CDK12 deficiency in RTECs affects the morphology of the urinary system

At the age of 10 weeks, $CDK12^{RTEC-/-}$ mice showed hydronephrosis, characterized by an enlarged urinary system, including hydronephrosis and bladder extension (Figures 3A–3D). Under higher magnification,

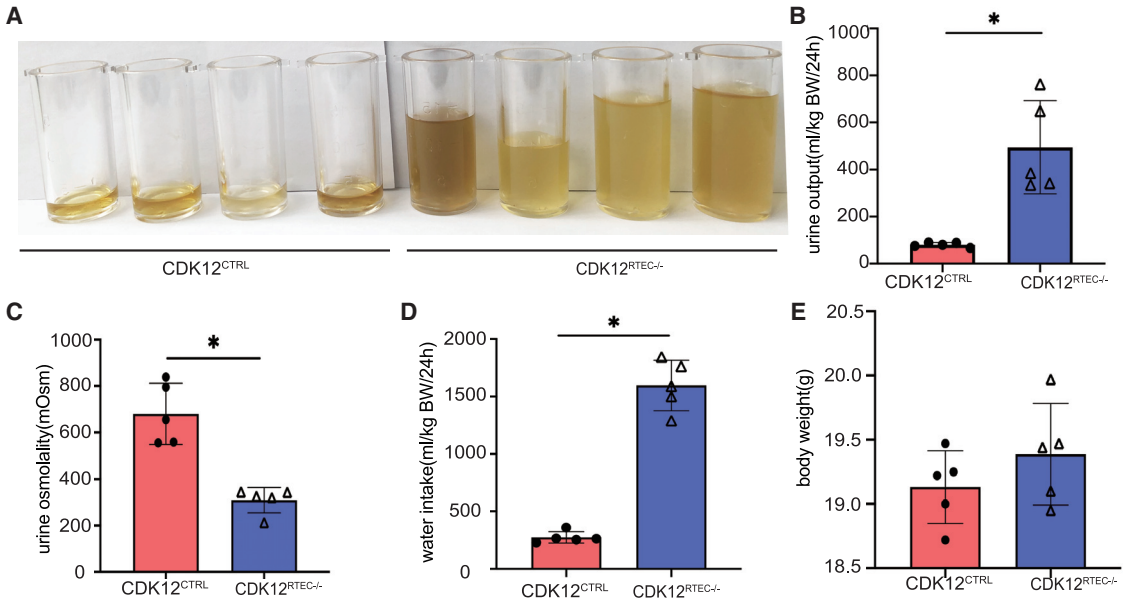

Figure 2. CDK12$^{RTEC-/-}$ mice display polyuria with low urine osmolality

(A and B) Representative urine appearance and urine volume of CDK12^{CTRL} and CDK12$^{RTEC-/-}$ mice. (C) Urine osmolality of CDK12^{CTRL} and CDK12$^{RTEC-/-}$ mice. (D) The volume of drinking water consumed by CDK12^{CTRL} and CDK12$^{RTEC-/-}$ mice. (E) Body weight of CDK12^{CTRL} and CDK12$^{RTEC-/-}$ mice. *p < 0.05 versus CDK12^{CTRL}, unpaired t-test, n = 5.

kidneys from CDK12$^{RTEC-/-}$ mice had severe renal tubule lumen dilation compared with the CDK12^{CTRL} mice (Figure 3E). CDK12 deficiency in RTECs induced mild tubulointerstitial fibrosis at week 10 without affecting the glomerular histology (Figures 3F and 3G). Consistently, CDK12$^{RTEC-/-}$ mice had higher blood urea nitrogen (BUN) and serum creatinine levels than CDK12^{CTRL} mice (Figures 3H and 3I). These data suggested that overloaded urination in CDK12$^{RTEC-/-}$ mice could cause hydronephrosis and mild tubulointerstitial fibrosis.

CDK12 deficiency in RTECs aggravates dehydration

Nephrogenic diabetes insipidus (NDI), the most common cause of polyuria, is induced by arginine vasopressin (AVP)-AVP receptor-aquaporin 2 (AQP2) axis defects.[14] CDK12$^{RTEC-/-}$ mice showed slightly elevated serum AVP levels compared with CDK12^{CTRL} mice, but the difference was not statistically significant (Figure 4A). Deprivation of drinking water for 24 h induced 20% body weight loss in the CDK12$^{RTEC-/-}$ mice (Figures 4B and 4C). However, both the urine volume and the urine osmolality showed no significant changes in CDK12$^{RTEC-/-}$ mice after water deprivation (Figures 4D and 4E). Concomitantly, water deprivation increased the serum sodium, potassium, and chloride levels of CDK12$^{RTEC-/-}$ mice but not CDK12^{CTRL} mice (Figures 4F–4H). In contrast, urine sodium, potassium, and chloride levels were significantly elevated in CDK12^{CTRL} mice but not CDK12$^{RTEC-/-}$ mice (Figures 4I–4K). These observations suggested that the CDK12$^{RTEC-/-}$ mice had defects in responding to antidiuretic signals.

AQP2 is the effector of AVP, and AQP2 loss-mediated water nonpermeability is a central component of NDI.[15] The *aqp2* mRNA level was unexpectedly increased in the kidneys of CDK12$^{RTEC-/-}$ mice under water deprivation (Figure 4L) as well as the AQP2 protein level (Figures 4M and 4N). Defects in AQP2 shuttling to the cell surface impairs the urine concentrating capacity.[16–18] Interestingly, the location of AQP2 in the membrane was unimpaired in CDK12$^{RTEC-/-}$ mice (Figure 4O). Collectively, these data indicated that the polyuria in CDK12$^{RTEC-/-}$ mice was not caused by the loss and/or abnormal distribution of AQP2.

Potential targets for CDK12 in RTECs

Gene expression analyses showed differential expression of 2,203 genes between CDK12^{CTRL} and CDK12 $^{RTEC-/-}$ mice. The data revealed that 1,059 of the genes were downregulated, and 1,144 were upregulated (Data S1). Gene ontology (GO) enrichment analysis of the downregulated genes revealed enrichment of genes associated with transmembrane transporter activity (Figure 5A). By computational mining of PubMed, we identified 11 genes, the deletion of which results in polyuria. The differential expression of those genes in our gene expression omnibus data was ranked. Interestingly, the cotransporter solute carrier family 12 member 1 (*Slc12a1*) and *aqp1* were significantly decreased in CDK12$^{RTEC-/-}$ versus CDK12^{CTRL} mice (Figures 5B and 5C). We performed RT-qPCR for the *Slc12a1* and *aqp1* genes and immunoblotting for Na-K-2Cl cotransporter 2 (NKCC2) (the protein encoded by the *Slc12a1* gene) and AQP1. There was a significant decline in *Slc12a1* mRNA and NKCC2 protein levels in CDK12$^{RTEC-/-}$ mice but no changes in the levels of *aqp1* mRNA and AQP1 protein (Figures 5D–5H). The immunohistochemical results further verified that the expression of NKCC2, but not AQP1, was decreased in the medulla of CDK12$^{RTEC-/-}$ mice

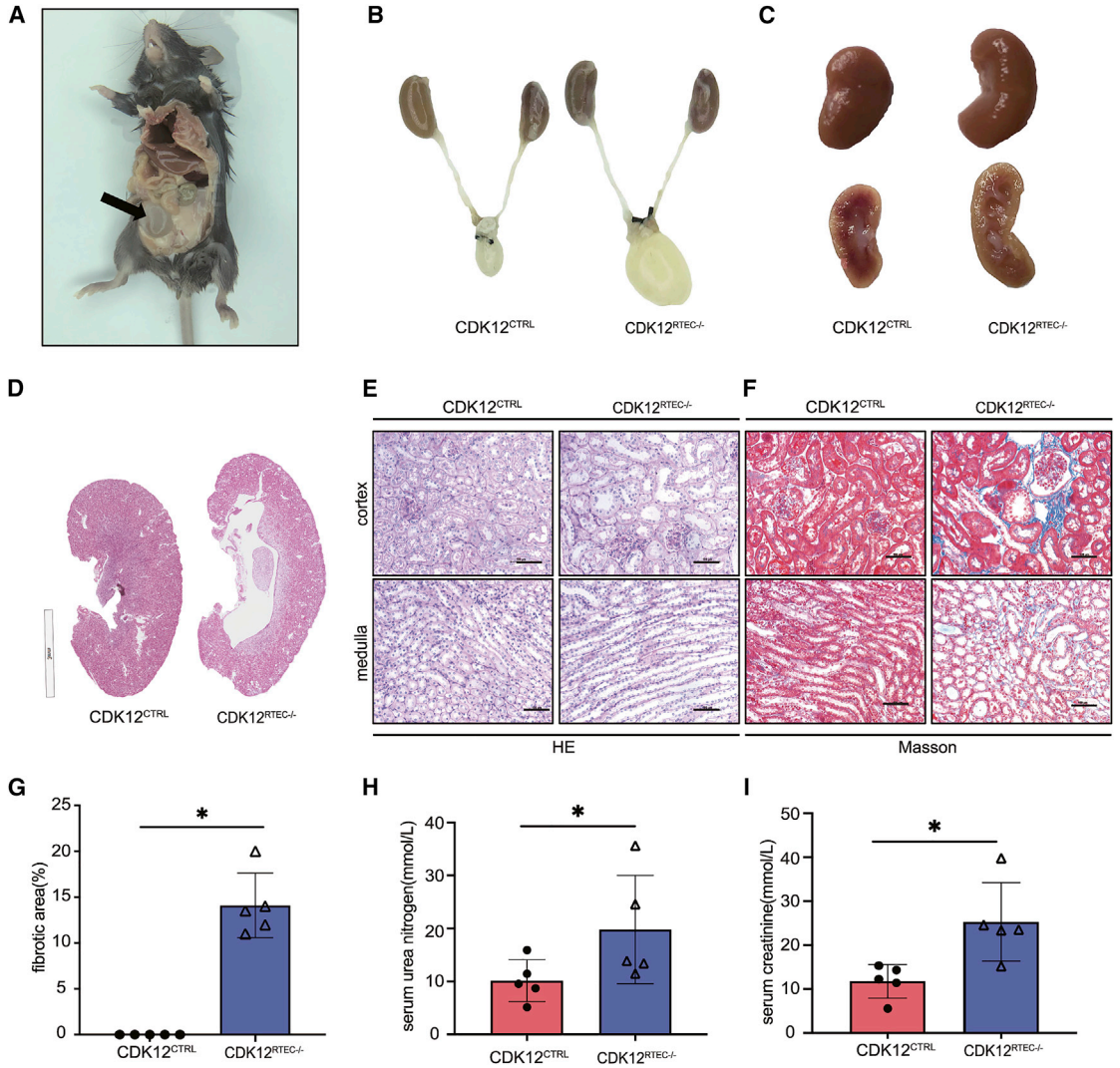

Figure 3. Morphological changes in the urinary system in CDK12$^{RTEC-/-}$ mice

(A) Representative images of enlarged bladders of CDK12$^{RTEC-/-}$ mice at 10 weeks old. Arrowheads indicate dilated urinary bladder. (B) Representative images of the urinary system in CDK12^{CTRL} and CDK12$^{RTEC-/-}$ mice at 10 weeks old. (C) Representative images of whole kidney and sagittal sections in CDK12^{CTRL} and CDK12$^{RTEC-/-}$ mice at 10 weeks old. (D) Representative images of H&E staining on sagittal sections in CDK12^{CTRL} and CDK12$^{RTEC-/-}$ mice at 10 weeks old. Scale bars, 3 mm. (E) Representative images of H&E staining and (F and G) Masson's trichrome staining in CDK12^{CTRL} and CDK12$^{RTEC-/-}$ mice at 10 weeks old Scale bars, 100 μm. (H) BUN and (I) creatinine levels in CDK12^{CTRL} and CDK12$^{RTEC-/-}$ mice at 10 weeks of age. *$p < 0.05$ versus CDK12^{CTRL}, unpaired t-test, n = 5.

compared with CDK12^{CTRL} mice (Figure 5I). Moreover, the expression of *SLC12A1* and NKCC2 significantly decreased in CDK12 small interfering RNA (siRNA)-treated HEK293 cells compared with controls (Figures 5J–5L). Thus, RTEC-specific CDK12 deficiency may induce renal concentration defects by inhibiting NKCC2 expression.

NKCC2 overexpression improved polyuria in CDK12$^{RTEC-/-}$ mice

To further confirm the causative effect of NKCC2 in CDK12 deficiency-induced polyuria, GFP-labeled NKCC2 overexpression lentivirus was administered to 4-week-old CDK12^{CTRL} and CDK12$^{RTEC-/-}$ mice. Urine samples were collected every week, and the mice were sacrificed at 6 weeks old (Figure 6A). Lentivirus injection successfully rescued renal NKCC2 expression after 2 weeks (Figures 6B–6E). The body weight increase of CDK12$^{RTEC-/-}$ mice was indistinguishable from that of CDK12^{CTRL} mice (Figure 6G). CDK12$^{RTEC-/-}$ mice exhibited a urine output reduction after 1 week of lentivirus injection and the change was more significant after 2 weeks (Figures 6F and 6H). Strikingly, NKCC2 overexpression lentivirus administration caused a fold increase in urinary sodium, chloride, and urine osmolality in CDK12$^{RTEC-/-}$ mice (Figures 6I–6L). Collectively, we concluded that NKCC2 downregulation was causing the urine concentration defect in CDK12$^{RTEC-/-}$ mice.

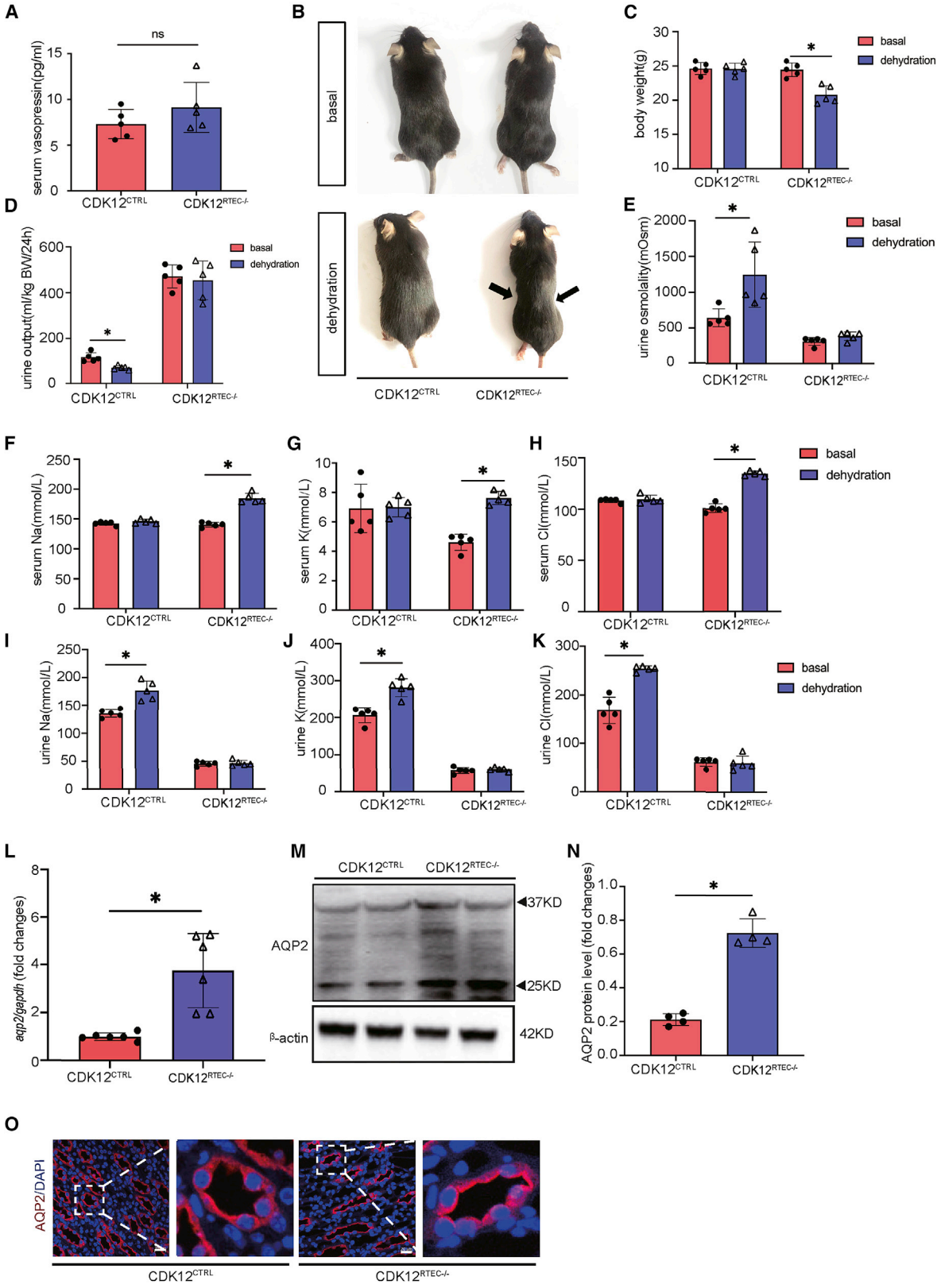

(legend on next page)

Knockout of CDK12 in RTECs increases intronic polyadenylation (IPA) and premature cleavage of the *slc12a1* gene

Previous reports have verified that CDK12 preferentially regulates the expression of long genes with high numbers of exons.[5] Here, we found a significant loss of genes featuring long genes and higher numbers of exons compared with the known transcript reference genome, especially in genes with more than 20 exons (Data S2). GO enrichment analysis of the significantly changed genes showed enrichment of genes associated with RNAPII-proximal-promoter-sequence-specific DNA binding and regulation, which were upregulated (Figure 7A). Concomitantly, RNAPII C-terminal domain (CTD) Ser2 and Ser5 phosphorylation was reduced in $CDK12^{RTEC-/-}$ mice. In an *in vitro* study, RNAPII CTD Ser2 and Ser5 phosphorylation was also decreased in siCDK12-treated HEK293 cells (Figures 7B–7H).

CDK12 regulates RNA splicing, cleavage, and polyadenylation.[19–21] Oxford Nanopore Technologies (ONT) were applied to detect the polyadenylation events and the transcript of *slc12a1* due to its ultra-long read length.[22] Compared with $CDK12^{CTRL}$ mice, the *slc12a1* gene in $CDK12^{RTEC-/-}$ mouse kidneys was enriched in intronic polyadenylation (IPA) events, but it lost the distal polyadenylation site and formed short *slc12a1* transcript variants (Figures 7I and 7J). Taken together, our data suggested that CKD12 knockout could cause an increase in *Slc12a1* gene IPA site usage, which resulted in *Slc12a1* gene truncated transcript production and NKCC2 downregulation.

DISCUSSION

In the present study, we generated a renal-tubular-specific CDK12 knockout (KO) mouse and demonstrated that CDK12 plays a critical role in maintaining renal water and electrolyte homeostasis by regulating *Slc12a1* gene transcription. CDK12 loss in RTECs reduced RNAPII CTD phosphorylation, increased IPA site usage, and formed truncated isoforms of the *Slc12a1* gene transcript, finally downregulating NKCC2.

NDI, the primary cause of polyuria, is linked to the effects of *AVPR2* or *AQP2* mutation in the collecting duct.[23,24] The collecting duct is the final concentration segment of the nephron, and its function depends on the availability and proper luminal side distribution of AQP2 water channels.[25] Interestingly, both vasopressin and AQP2 were slightly increased in the $CDK12^{RTEC-/-}$ mouse kidney, even though the vasopressin changes did not reach statistical significance. In addition, AQP2 typically aggregated at the luminal side of the collecting duct in $CDK12^{RTEC-/-}$ mice. These data suggested that the polyuria in $CDK12^{RTEC-/-}$ mice is distinct from that of NDI. AQP2 accumulation is possibly the outcome of the compensatory response under hyposthenuria.

NKCC2 is an integral membrane protein restricted to the apical membrane of the thick ascending limbs (TALs) of Henle's loop, which is water impermeable. NKCC2 mediates the cotranslocation of Na^+, K^+, and 2 Cl^- ions through the apical membrane of TALs.[26] The major constituent of the osmotic gradient is NaCl. NaCl absorbed by NKCC2 enriches interstitial osmolality and fuels the countercurrent multiplication mechanism.[27,28] To produce concentrated urine, the collecting duct, in a second step, has to allow water to be reabsorbed through AQP2 and therefore equilibration of the luminal osmolality to the basolateral osmolality. The absence of salt transport across NKCC2 in TALs prevents the establishment of the normal osmotic gradient, which is necessary for urine concentration.[28,29] Similar to $NKCC2^{-/-}$ mice and Na-K-2Cl transport inhibitor furosemide-treated wild-type mice, $CDK12^{RTEC-/-}$ mice manifested NKCC2 reduction, dissolved medullary hyperosmotic, and polyuria (Figures 2A and 5F).[30] The effect of the NKCC2 reduction responsible for the polyuria in $CDK12^{RTEC-/-}$ mice was further confirmed by our rescue experiments: NKCC2 overexpression reduced the urine output of $CDK12^{RTEC-/-}$ mice (Figure 6).

NKCC2 is encoded by the *Slc12a1* gene, located on chromosome 2, containing 29 exons with a full length of 77 kb.[26] Consistent with previous studies, CDK12 deficiency preferentially affects long genes with high numbers of exons.[5] It has been reported that CDK12 depletion decreases RNAPII CTD phosphorylation and lowers the RNAPII elongation rates.[20,31] Our data showed that CDK12 loss reduced RNAPII CTD Ser2 and Ser5 phosphorylation. Ser5 phosphorylation is required for establishing pausing, and Ser2 phosphorylation is necessary for coupling transcription to mRNA processing.[32] Meanwhile, the accumulation of the RNAPII-proximal-promoter-sequence-specific DNA binding genes in $CDK12^{RTEC-/-}$ mouse kidneys indicated that the RNAPII density increased upstream and less RNAPII entered productive elongation.[33,34] These results suggested that CDK12 KO induced downregulation of RNAPII CTD Ser2 and Ser5 phosphorylation may slow *Slc12a1* gene transcriptional elongation dynamics.

Because Cdk12-dependent RNAPII CTD Ser2 phosphorylation suppresses IPA site usage, CDK12-KO-induced RNAPII CTD Ser2 and Ser5 phosphorylation downregulation may result in IPA events in the *Slc12a1* gene.[20,35] ONT could offer the ability to directly access full-length transcript data that can more accurately reflect

Figure 4. Changes in $CDK12^{RTEC-/-}$ mice under dehydration

(A) Plasma AVP levels in $CDK12^{CTRL}$ and $CDK12^{RTEC-/-}$ mice at 10 weeks old. (B) Representative images of mice under water provision and deprivation for 24 h; arrowheads indicate dehydration. (C) Body weight changes before and after 24 h of water deprivation in $CDK12^{CTRL}$ and $CDK12^{RTEC-/-}$ mice. (D) Urine output and (E) urine osmolality of $CDK12^{CTRL}$ and $CDK12^{RTEC-/-}$ mice before and after 24 h of water deprivation. (F) Serum sodium, (G) potassium, (H) chloride and (I) urine sodium, (J) potassium, and (K) chloride in $CDK12^{CTRL}$ and $CDK12^{RTEC-/-}$ mice before and after 24 h of water deprivation. Data are the means ± SE, n = 5. (L) Relative *aqp2* gene expression levels in $CDK12^{CTRL}$ and $CDK12^{RTEC-/-}$ mouse kidneys, n = 6. (M and N) Western blot analysis of glycosylated (arrowhead, 37 kDa) and nonglycosylated (arrowhead, 25 kDa) AQP2 in kidney tissues. Data are presented as the means ± SE, n = 4. (O) Representative confocal images showing the changes in AQP2 in tubules in paraffin-embedded kidney sections. Scale bar, 20 μm. *$p < 0.05$ versus $CDK12^{CTRL}$, unpaired t-test, n = 5.

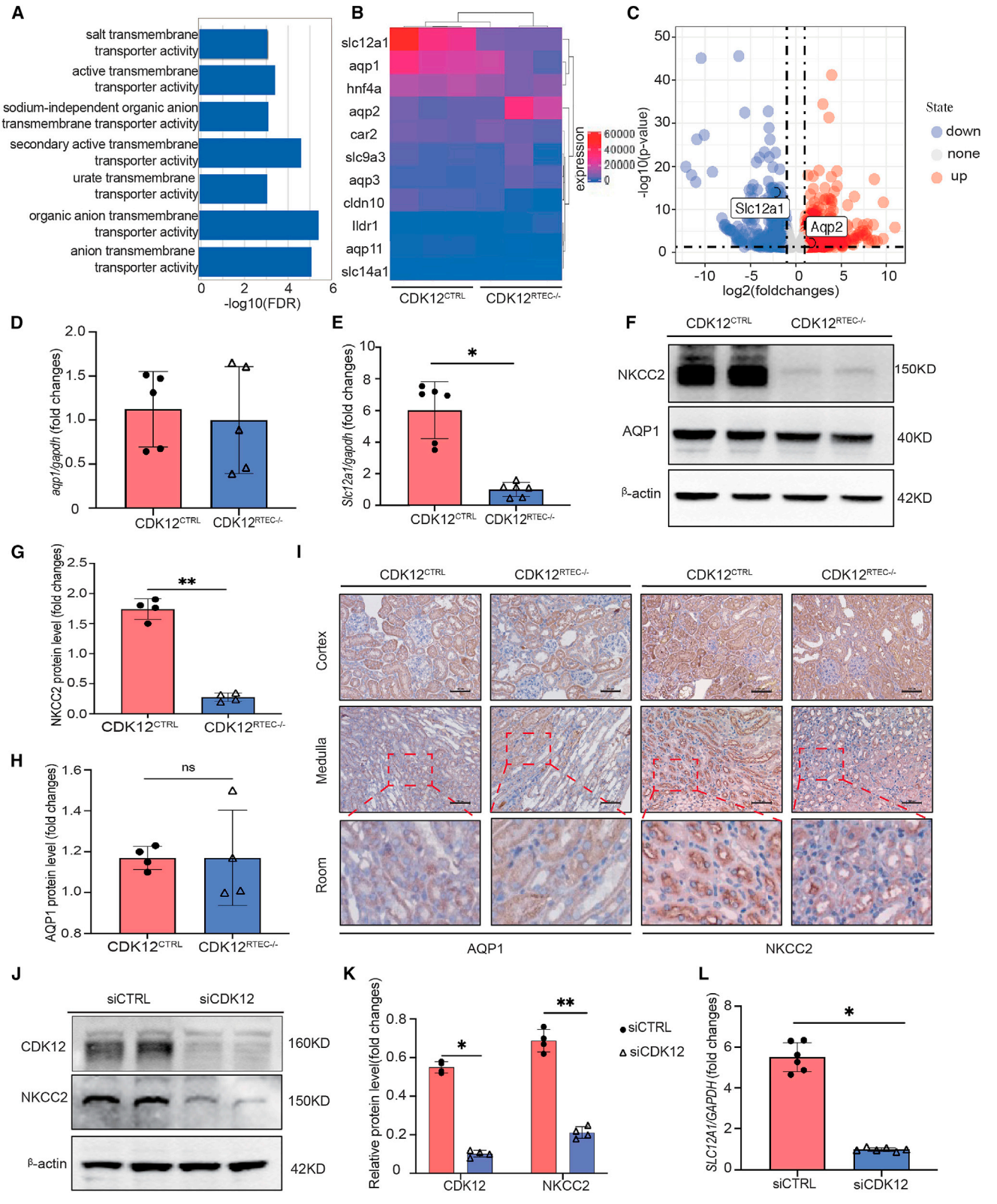

(legend on next page)

transcriptome information and has significant advantages in identifying novel RNA molecules and complex isoforms.[36,37] In this study, ONT RNA sequencing (RNA-seq) data indicated that the *Slc12a1* gene was enriched in the frequency of proximal IPA events but lost distal polyadenylation in CDK12$^{RTEC-/-}$ mice. As reported before, the increased *Slc12a1* gene proximal IPA site usage decreased the splicing efficiency and then increased the cleavage activity, which was directly strengthened by the accumulation of *Slc12a1* short truncated isoforms.[38,39]

The kidney histological findings in CDK12$^{RTEC-/-}$ mice showed obvious hydronephrosis and mild tubulointerstitial fibrosis. Previously, many studies have suggested that tubulointerstitial inflammation and fibrosis predict a detrimental outcome of chronic kidney disease.[40–44] The tubulointerstitial lesion of CDK12$^{RTEC-/-}$ mice may be the result of the long-term elevation of renal pelvis pressure and activation of profibrotic factors mediated by CDK12 KO.

Since the development of CDK12 inhibitors, they have been increasingly used in the treatment of cancers.[5,45] However, renal function decline as well as water electrolyte disorders, including hyponatremia, hypochloridemia, hypokalemia, and hypotension (Table S1), have been repeatedly reported in clinical trials of CDK12 inhibitors, while the potential mechanism is not understood. Our present study provides a novel molecular mechanism for the critical renal adverse effects induced by CDK12 inhibitors, implying that special care should be taken in regard to water electrolyte disorders and kidney dysfunction when CDK12 inhibitors are used to treat cancers.

In summary, CDK12 activity is essential for maintaining renal homeostasis by regulating NKCC2 transcription, and CDK12 deficiency in RTECs causes urine concentration defects due to premature cleavage of the *slc12a1* gene. Therefore, when CDK12 inhibitors are applied in patients with cancers, it is important to be aware that fluid and electrolyte disturbances should be prevented to avoid kidney damage and critical clinical situations.

MATERIALS AND METHODS

Cell culture

HEK293 cells were obtained from ATCC (ATCC CRL-1573). HEK293 cells were grown in DMEM supplemented with 10% fetal calf serum and 2 mM L-glutamine at 37°C and 5% CO_2.

Transfection of CDK12-siRNA into HEK293 cells

To downregulate the expression of CDK12 in HEK293 cells, transfections were performed using Lipofectamine 3000 reagent (Invitrogen) with si-CDK12 (Hanheng). Briefly, a total of 5 ng of siRNA and 2 μL of Lipofectamine 3000 were mixed with Opti-MEM for the transfection of approximately 8×10^6 cells. The cells were harvested 48 h after transfection.

Generation of CDK12$^{RTEC-/-}$ mice

Renal-tubular-specific CDK12$^{RTEC-/-}$ mice were generated by crossbreeding CDK12$^{flox/flox}$ with cdh16-*Cre*. Before phenotypic analyses, the colony was backcrossed onto a pure C57BL/6J genetic background for more than seven generations. Ten-week-old mice were subjected to analysis. An almost equal ratio of male to female mice was used in our experiments. The 24 h urine and drinking water were measured using a metabolic cage, and osmolality was measured by SRL. Plasma AVP was quantified with a competitive enzyme-linked immunoassay (Arg-Vasopressin ELISA Kit, Cusabio Life Sciences). Blood samples were collected from the mice and analyzed using the i-STAT 1 analyzer (Abbott). All animal experiments were performed in accordance with standard guidelines for the care and use of laboratory animals and approved by our institutional animal care and use committee.

In vivo virus transduction

In vivo virus transduction to express *Slc12a1* in CDK12 KO mice was performed as described previously with slight modifications.[46] Four-week-old mice (weighing 15 to 16 g) were anesthetized with pentobarbital sodium (50 mg/kg, Sigma-Aldrich) by intraperitoneal injection, and then a 31G needle was inserted at the lower pole of the bilateral kidneys parallel to the long axis and was carefully pushed toward the upper pole. As the needle was slowly removed, 50 μL of filter-purified lentivirus cocktail (EGFP or EGFP-slc12a1, ~2×10^6 IU/μL) was injected into each kidney. The 24 h urine was collected at 1 and 2 weeks after virus injection.

Kidney histology and quantification

Kidneys were fixed with 4% formaldehyde, embedded in paraffin, and sectioned to 4-mm thickness. Renal sections were used for H&E and Masson's trichrome staining. The results were averaged for each mouse. At least five random tissue sections per mouse were assessed by Masson's trichrome staining to evaluate interstitial fibrosis. Tissue fibrosis as defined by blue staining was scored by three experienced observers blinded to the experimental conditions, and the average values of the fibrosis scores were reported.

Figure 5. CDK12$^{RTEC-/-}$ mice exhibit a reduction in NKCC2 in the kidney

(A) GO enrichment analysis of downregulated genes in CDK12$^{RTEC-/-\ mice}$ compared with CDK12^{CTRL} mice. (B) Heatmap showing polyuria-related gene expression from RNA-seq data. (C) Log2 fold change (FC) gene expression volcano plots for CDK12^{CTRL} and CDK12$^{RTEC-/-}$ mouse kidneys. The *Slc12a1* gene and *aqp2* gene are labeled. Genes exhibiting a log2FC of >2 (red) or <−2 (blue) with an adjusted p <0.01 are highlighted. (D) Relative *aqp1* gene expression levels in CDK12^{CTRL} and CDK12$^{RTEC-/-}$ mouse kidneys, n = 6. (E) Relative *Slc12a1* gene expression levels in CDK12^{CTRL} and CDK12$^{RTEC-/-}$ mouse kidneys, n = 6. (F–H) Western blot analysis of AQP1 and NKCC2 in CDK12^{CTRL} and CDK12$^{RTEC-/-}$ mice, n = 4. *p < 0.05 versus CDK12^{CTRL}, unpaired *t*-test. (I) Representative immunohistochemical staining images showing the changes in AQP1 and NKCC2 in the cortex and medulla in paraffin-embedded kidney sections. Scale bars, 100 μm. (J and K) Western blot analysis of CDK12 and NKCC2 in HEK293 cells transfected with siCDK12 and control siRNA, n = 4. (L) Relative *SLC12A1* gene expression level in HEK293 cells transfected with siCDK12 and control siRNA, n = 6. *p < 0.05, < 0.05, **p < 0.01 versus the control siRNA treated HEK293 cells, unpaired t-test.

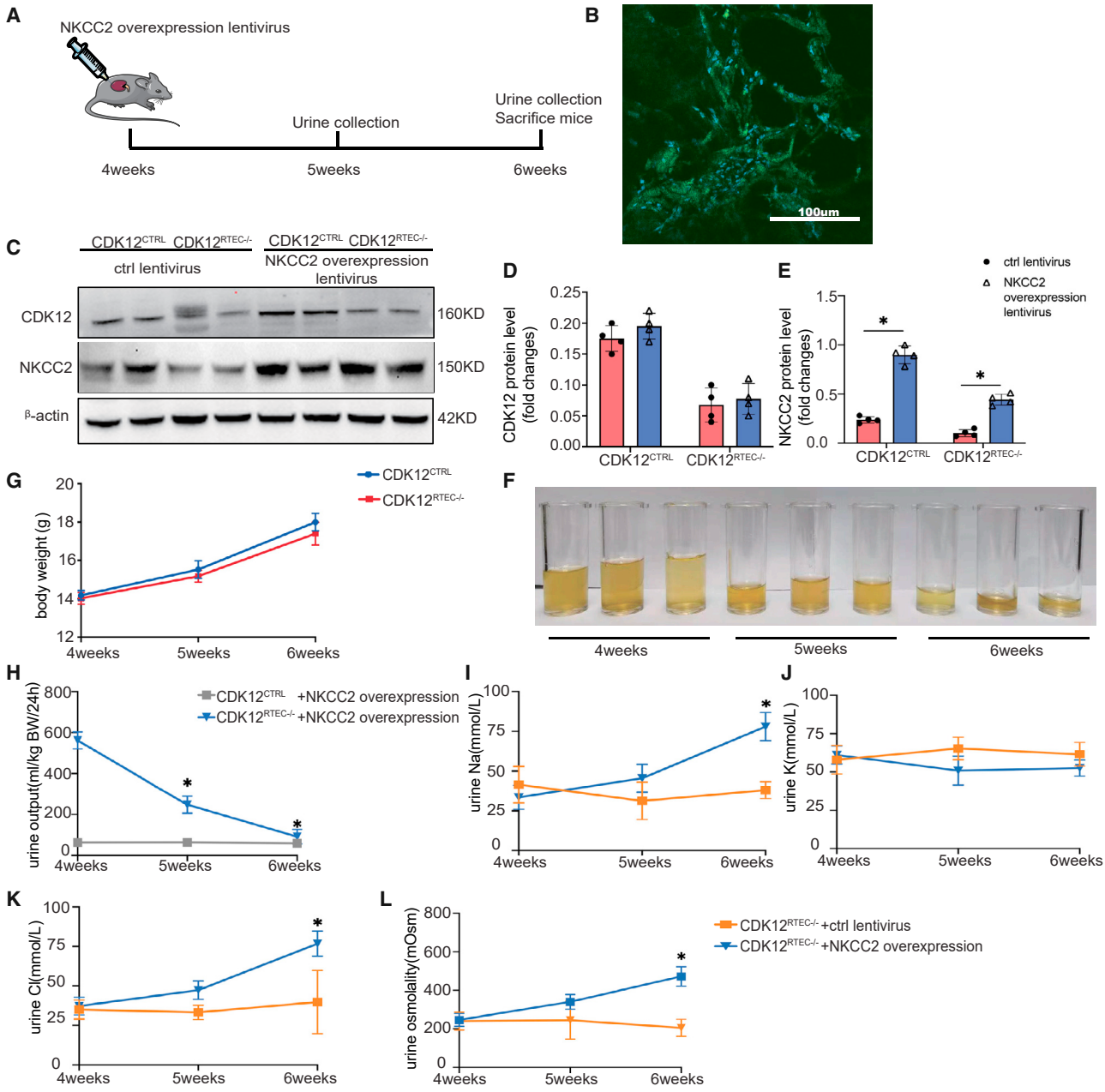

Figure 6. Overexpression of NKCC2 rescues CDK12$^{RTEC-/-}$ mouse polyuria

(A) Schematic diagram of the experimental design. Briefly, mouse bilateral kidneys were administered NKCC2 overexpressing lentivirus at 4 weeks old, and urine was collected every 1 week for 2 weeks after lentivirus injection. (B) Representative images of GFP fluorescence in the kidney. Scale bar, 100 μm. (C–E) Western blot analysis of CDK12 and NKCC2 in kidney tissues, n = 4. *p < 0.05 versus the control lentivirus injection. (G) Growth curve for CDK12^{CTRL} and CDK12$^{RTEC-/-}$ mice after NKCC2 overexpressing lentivirus injection. (F and H) Representative appearance and volume of urine after lentivirus injection (I) urine sodium, (J) potassium, (K) chloride, and (L) urine osmolality after lentivirus injection, n = 4. Data are presented as the means ± SD. *p < 0.05 versus the 4 weeks CDK12$^{RTEC-/-}$ mice, one-way ANOVA.

Quantitative real-time PCR assay

Total RNA from cells or kidneys was extracted using TRIzol (Invitrogen), and complementary DNA was synthesized using a PrimeScript RT reagent kit (Takara Bio). Reverse transcript quantitative PCR (RT-qPCR) was performed using a real-time PCR system (Bio-Rad). The primer sequences are listed in Table S2.

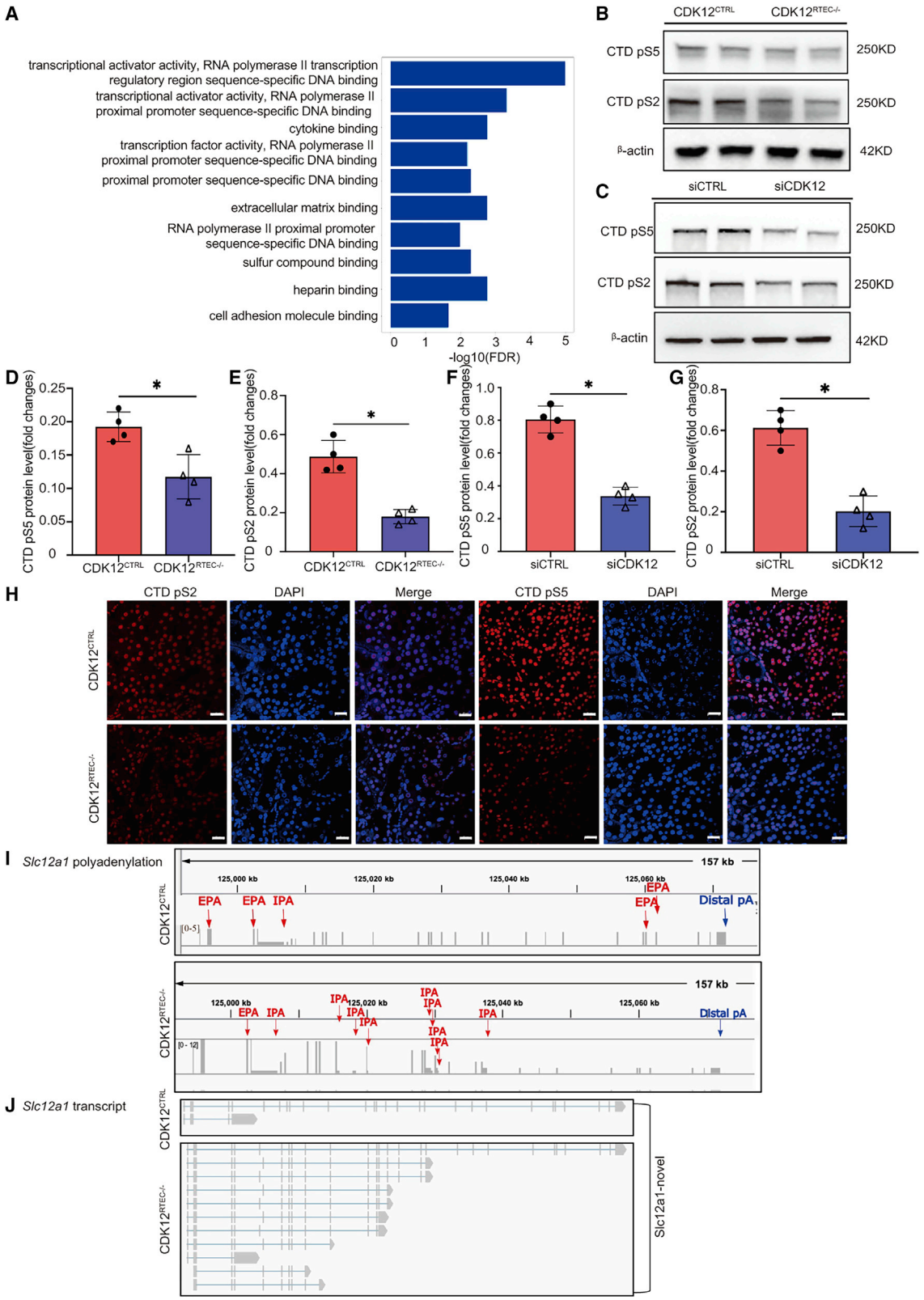

(legend on next page)

Western blot

The protein lysates from HEK293 cells and kidney tissues were prepared following standard protocols, and the protein content was determined using a BCA protein assay kit (Thermo Fisher Scientific). Then, the protein samples were separated by Bis-Tris gel (Invitrogen) and transferred onto polyvinylidene difluoride membranes (Millipore) using a wet transfer system. Membranes were blocked in 5% BSA in TBS-T (Tris-buffered saline with Tween 20) for 1 h at room temperature and were incubated with primary antibodies overnight at 4°C. The primary antibodies used were anti-AQP2 (ab199975, Abcam; 1:1,000 dilution), anti-Slc12a1 (Proteintech, 18970-1-ap; 1:1,000 dilution), anti-RNAP II CTD repeat YSPTSPS (phospho S2) (ab5095, Abcam; 1:3,000 dilution), anti-RNAP II CTD repeat YSPTSPS (phospho S5) (ab5131, Abcam; 1:3,000 dilution), anti-Rpb1 NTD (14958, Cell Signaling Technology; 1:3,000 dilution), and anti-β-actin (sc-81178, Santa Cruz Biotechnology; 1:40,00 dilution). Then, the membranes were washed and incubated with HRP-conjugated secondary antibodies for 2 h at room temperature, and the signals were detected using an enhanced chemiluminescence advanced system (GE Healthcare).

Immunohistochemistry and immunofluorescence staining

For immunostaining, samples were stained using anti-AQP1 (sc-25287; Santa Cruz Biotechnology; 1:400 dilution) and anti-Slc12a1 (Proteintech, 18970-1-ap; 1:500 dilution) and then analyzed using a streptavidin peroxidase detection system (Maixin) according to the manufacturer's protocol. Diaminobenzidine (DAB) (Maixin) was used as the horseradish peroxidase (HRP)-specific substrate.

For immunofluorescence staining, formaldehyde-fixed kidney sections were incubated with primary antibodies, including anti-AQP2 (ab199975, Abcam; 1:500 dilution), anti-RNAPII pSer2, (ab5095, Abcam; 1:1,000 dilution), anti-RNAPII pSer5 (ab5131, Abcam; 1:1,000 dilution), and anti-CDK12 (ab2346, Abcam; 1:50 dilution), and then incubated with secondary antibodies. Cell nuclei were stained with DAPI. Immunostained samples were visualized under a confocal microscope (LSM 880NLO, Zeiss).

RNA-seq and genome-wide transcriptome analysis

RNA from the kidneys of mice was prepared for RNA-seq (three biological replicates for each group). RNA-seq experiments were performed by Novogene (Beijing, China). Briefly, total RNA was isolated from fresh kidney tissue using TRIzol (Invitrogen). Following the manufacturer's recommendations, sequencing libraries were generated using the NEBNext Ultra RNA Library Prep Kit for Illumina (New England Biolabs, USA), and index codes were added to attribute the sequences to each sample. The library preparations were sequenced on an Illumina HiSeq platform, and 150 bp paired-end reads were generated. Reference genome and gene model annotation files were downloaded from the genome website directly. HTSeq v.0.6.0 was used to count the read numbers mapped to each gene. Differential expression analysis of the two conditions was performed using the edgeR R package (v.3.18.1). The p values were adjusted using the Benjamini-Hochberg method.[47]

RNA-seq by Oxford Nanopore Technologies (ONT)

The same RNA used for RNA-seq was used for ONT RNA-seq, and the ONT RNA-seq experiments were performed by Novogene (Beijing, China). Oxford PromethION 2D amplicon libraries were generated according to the ONT community protocol using the library preparation kit SQK-LSK109 and sequenced on R9 flow cells to generate fast5 files. Coding-Non-Coding-Index profiles were set as default parameters. hmmscan software was used for the protein family (Pfam) database analysis, and BLAST software was used for the NCBI nonredundant nucleotide sequence database analysis. Structure annotation was performed using GffCompare to identify known and novel transcripts.[48]

Statistical analysis

Data are expressed as the means ± SD. Statistical analysis was performed using an unpaired t-test or one-way ANOVA. $p < 0.05$ was considered statistically significant.

SUPPLEMENTAL INFORMATION

Supplemental information can be found online at https://doi.org/10.1016/j.ymthe.2022.05.012.

ACKNOWLEDGMENTS

This work was supported by grants from the National Natural Science Foundation of China (82030024 and 81720108007) to B.-C.L., National Natural Science Foundation of China (82070735) to B.W., National Natural Science Foundation of China (81900623) to U.W., National Natural Science Foundation of China (82122011) to L.-L.L., and the Natural Science Foundation of Jiangsu Province (BK20181487) B.W. This research was supported by additional grants from the National Key Research Programme of the Ministry of Science and Technology (2018YFC1314000) to B.-C.L.

AUTHOR CONTRIBUTIONS

Conceptualization: Y.W., B.W., and B.-C.L.; methodology: Y.W., B.W., W.-J.N., and Y.-L.Z.; animal experiments: Y.W., J.-Y.C., D.Y., and Q.Y.; pathology analysis: L.-L.L., T.-T.T., and W.J.; supervision:

Figure 7. Mechanism by which CKD12 regulates NKCC2 expression

(A) GO enrichment analysis of upregulated genes in the molecular function category in $CDK12^{RTEC-/-}$ mice compared with $CDK12^{CTRL}$ mice. (B, D, and E) Western blot analysis of RNAPII CTD pSer2 and pSer5 in $CDK12^{CTRL}$ and $CDK12^{RTEC-/-}$ mouse kidneys,n = 4, *p < 0.05 versus the $CDK12^{CTRL}$ mice, unpaired t-test.(C, F, and G) Western blot analysis of RNAPII CTD pSer2 and pSer5 in HEK293 cells transfected with siCKD12 and control siRNA n = 4, *p < 0.05 versus the control siRNA treated HEK293 cells, unpaired -test.< 0.05 versus the control siRNA treated HEK293 cells, unpaired t-test. (H) Representative confocal images show the changes in RNAPII pSer2 and pSer5 in the nuclei of tubules in paraffin-embedded kidney sections. Scale bars, 20 μm. (I) ONT RNA-seq read density across the *Slc12a1* gene locus depicting the annotated polyadenylation signal in $CDK12^{CTRL}$ and $CDK12^{RTEC-/-}$ mouse kidneys. EPA, exon polyadenylation; IPA, intronic polyadenylation; Distal pA, distal polyadenylation. (J) ONT RNA-seq read transcript of the *Slc12a1* gene and its variants in $CDK12^{CTRL}$ and $CDK12^{RTEC-/-}$ mouse kidneys.

L.-L.L. and Y.W.; writing—original draft: Y.W. and B.W.; writing—review & editing: B.W., Y.W., and B.-C.L.

DECLARATION OF INTERESTS

None.

REFERENCES

1. Ko, T.K., Kelly, E., and Pines, J. (2001). CrkRS: a novel conserved Cdc2-related protein kinase that colocalises with SC35 speckles. J. Cell Sci. *114*, 2591–2603.
2. Dar, A.A., Nosrati, M., Bezrookove, V., de Semir, D., Majid, S., Thummala, S., Sun, V., Tong, S., Leong, S.P.L., Minor, D., et al. (2015). The role of BPTF in melanoma progression and in response to BRAF-targeted therapy. J. Natl. Cancer Inst. *107*. https://doi.org/10.1093/jnci/djv034.
3. Carter, S.L., Cibulskis, K., Helman, E., McKenna, A., Shen, H., Zack, T., Laird, P.W., Onofrio, R.C., Winckler, W., Weir, B.A., et al. (2012). Absolute quantification of somatic DNA alterations in human cancer. Nat. Biotechnol. *30*, 413–421. https://doi.org/10.1038/nbt.2203.
4. Fusco, N., Geyer, F.C., De Filippo, M.R., Martelotto, L.G., Ng, C.K.Y., Piscuoglio, S., Guerini-Rocco, E., Schultheis, A.M., Fuhrmann, L., Wang, L., et al. (2016). Genetic events in the progression of adenoid cystic carcinoma of the breast to high-grade triple-negative breast cancer. Mod. Pathol. *29*, 1292–1305. https://doi.org/10.1038/modpathol.2016.134.
5. Blazek, D., Kohoutek, J., Bartholomeeusen, K., Johansen, E., Hulinkova, P., Luo, Z., Cimermancic, P., Ule, J., and Peterlin, B.M. (2011). The Cyclin K/Cdk12 complex maintains genomic stability via regulation of expression of DNA damage response genes. Genes Dev. *25*, 2158–2172. https://doi.org/10.1101/gad.16962311.
6. Bajrami, I., Frankum, J.R., Konde, A., Miller, R.E., Rehman, F.L., Brough, R., Campbell, J., Sims, D., Rafiq, R., Hooper, S., et al. (2014). Genome-wide profiling of genetic synthetic lethality identifies CDK12 as a novel determinant of PARP1/2 inhibitor sensitivity. Cancer Res. *74*, 287–297. https://doi.org/10.1158/0008-5472.Can-13-2541.
7. Li, Y., Zhang, H., Li, Q., Zou, P., Huang, X., Wu, C., and Tan, L. (2020). CDK12/13 inhibition induces immunogenic cell death and enhances anti-PD-1 anticancer activity in breast cancer. Cancer Lett. *495*, 12–21. https://doi.org/10.1016/j.canlet.2020.09.011.
8. Wang, C., Wang, H., Lieftink, C., du Chatinier, A., Gao, D., Jin, G., Jin, H., Beijersbergen, R.L., Qin, W., and Bernards, R. (2020). CDK12 inhibition mediates DNA damage and is synergistic with sorafenib treatment in hepatocellular carcinoma. Gut *69*, 727–736. https://doi.org/10.1136/gutjnl-2019-318506.
9. Johnson, S.F., Cruz, C., Greifenberg, A.K., Dust, S., Stover, D.G., Chi, D., Primack, B., Cao, S., Bernhardy, A.J., Coulson, R., et al. (2016). CDK12 inhibition reverses De Novo and acquired PARP inhibitor resistance in BRCA wild-type and mutated models of triple-negative breast cancer. Cell Rep. *17*, 2367–2381. https://doi.org/10.1016/j.celrep.2016.10.077.
10. Johannes, J.W., Denz, C.R., Su, N., Wu, A., Impastato, A.C., Mlynarski, S., Varnes, J.G., Prince, D.B., Cidado, J., Gao, N., et al. (2018). Structure-based design of selective noncovalent CDK12 inhibitors. ChemMedChem *13*, 231–235. https://doi.org/10.1002/cmdc.201700695.
11. Pattaro, C., Köttgen, A., Teumer, A., Garnaas, M., Böger, C.A., Fuchsberger, C., Olden, M., Chen, M.H., Tin, A., Taliun, D., et al. (2012). Genome-wide association and functional follow-up reveals new loci for kidney function. PLoS Genet. *8*, e1002584. https://doi.org/10.1371/journal.pgen.1002584.
12. Juan, H.C., Lin, Y., Chen, H.R., and Fann, M.J. (2016). Cdk12 is essential for embryonic development and the maintenance of genomic stability. Cell Death Differ. *23*, 1038–1048. https://doi.org/10.1038/cdd.2015.157.
13. Shao, X., Johnson, J.E., Richardson, J.A., Hiesberger, T., and Igarashi, P. (2002). A minimal Ksp-cadherin promoter linked to a green fluorescent protein reporter gene exhibits tissue-specific expression in the developing kidney and genitourinary tract. J. Am. Soc. Nephrol. *13*, 1824–1836. https://doi.org/10.1097/01.asn.0000016443.50138.cd.
14. Lloyd, D.J., Hall, F.W., Tarantino, L.M., and Gekakis, N. (2005). Diabetes insipidus in mice with a mutation in aquaporin-2. PLoS Genet. *1*, e20. https://doi.org/10.1371/journal.pgen.0010020.
15. Christ-Crain, M., Bichet, D.G., Fenske, W.K., Goldman, M.B., Rittig, S., Verbalis, J.G., and Verkman, A.S. (2019). Diabetes insipidus. Nat. Rev. Dis. Primers *5*, 54. https://doi.org/10.1038/s41572-019-0103-2.
16. Laszczyk, A.M., Higashi, A.Y., Patel, S.R., Johnson, C.N., Soofi, A., Abraham, S., and Dressler, G.R. (2020). Pax2 and Pax8 proteins regulate urea transporters and aquaporins to control urine concentration in the adult kidney. J. Am. Soc. Nephrol. *31*, 1212–1225. https://doi.org/10.1681/asn.2019090962.
17. Whiting, J.L., Ogier, L., Forbush, K.A., Bucko, P., Gopalan, J., Seternes, O.M., Langeberg, L.K., and Scott, J.D. (2016). AKAP220 manages apical actin networks that coordinate aquaporin-2 location and renal water reabsorption. Proc. Natl. Acad. Sci. U S A *113*, E4328–E4337. https://doi.org/10.1073/pnas.1607745113.
18. Li, S., Qiu, M., Kong, Y., Zhao, X., Choi, H.J., Reich, M., Bunkelman, B.H., Liu, Q., Hu, S., Han, M., et al. (2018). Bile acid G protein-coupled membrane receptor TGR5 modulates aquaporin 2-mediated water homeostasis. J. Am. Soc. Nephrol. *29*, 2658–2670. https://doi.org/10.1681/asn.2018030271.
19. Krajewska, M., Dries, R., Grassetti, A.V., Dust, S., Gao, Y., Huang, H., Sharma, B., Day, D.S., Kwiatkowski, N., Pomaville, M., et al. (2019). CDK12 loss in cancer cells affects DNA damage response genes through premature cleavage and polyadenylation. Nat. Commun. *10*, 1757. https://doi.org/10.1038/s41467-019-09703-y.
20. Dubbury, S.J., Boutz, P.L., and Sharp, P.A. (2018). CDK12 regulates DNA repair genes by suppressing intronic polyadenylation. Nature *564*, 141–145. https://doi.org/10.1038/s41586-018-0758-y.
21. Chirackal Manavalan, A.P., Pilarova, K., Kluge, M., Bartholomeeusen, K., Rajecky, M., Oppelt, J., Khirsariya, P., Paruch, K., Krejci, L., Friedel, C.C., and Blazek, D. (2019). CDK12 controls G1/S progression by regulating RNAPII processivity at core DNA replication genes. EMBO Rep. *20*, e47592. https://doi.org/10.15252/embr.201847592.
22. Zhang, S., Li, R., Zhang, L., Chen, S., Xie, M., Yang, L., Xia, Y., Foyer, C.H., Zhao, Z., and Lam, H.M. (2020). New insights into Arabidopsis transcriptome complexity revealed by direct sequencing of native RNAs. Nucleic Acids Res. *48*, 7700–7711. https://doi.org/10.1093/nar/gkaa588.
23. Bockenhauer, D., and Bichet, D.G. (2015). Pathophysiology, diagnosis and management of nephrogenic diabetes insipidus. Nat. Rev. Nephrol. *11*, 576–588. https://doi.org/10.1038/nrneph.2015.89.
24. Su, W., Cao, R., Zhang, X.Y., and Guan, Y. (2020). Aquaporins in the kidney: physiology and pathophysiology. Am. J. Physiol. Renal Physiol. *318*. F193-f203. https://doi.org/10.1152/ajprenal.00304.2019.
25. Noda, Y., Sohara, E., Ohta, E., and Sasaki, S. (2010). Aquaporins in kidney pathophysiology. Nat. Rev. Nephrol. *6*, 168–178. https://doi.org/10.1038/nrneph.2009.231.
26. Marcoux, A.A., Tremblay, L.E., Slimani, S., Fiola, M.J., Mac-Way, F., Garneau, A.P., and Isenring, P. (2021). Molecular characteristics and physiological roles of Na(+) -K(+) -Cl(-) cotransporter 2. J. Cell Physiol. *236*, 1712–1729. https://doi.org/10.1002/jcp.29997.
27. Kaplan, M.R., Plotkin, M.D., Lee, W.S., Xu, Z.C., Lytton, J., and Hebert, S.C. (1996). Apical localization of the Na-K-Cl cotransporter, rBSC1, on rat thick ascending limbs. Kidney Int. *49*, 40–47. https://doi.org/10.1038/ki.1996.6.
28. Greger, R. (1985). Ion transport mechanisms in thick ascending limb of Henle's loop of mammalian nephron. Physiol. Rev. *65*, 760–797. https://doi.org/10.1152/physrev.1985.65.3.760.
29. Gong, Y., Himmerkus, N., Sunq, A., Milatz, S., Merkel, C., Bleich, M., and Hou, J. (2017). ILDR1 is important for paracellular water transport and urine concentration mechanism. Proc. Natl. Acad. Sci. U S A *114*, 5271–5276. https://doi.org/10.1073/pnas.1701006114.
30. Takahashi, N., Chernavvsky, D.R., Gomez, R.A., Igarashi, P., Gitelman, H.J., and Smithies, O. (2000). Uncompensated polyuria in a mouse model of Bartter's syndrome. Proc. Natl. Acad. Sci. U S A *97*, 5434–5439. https://doi.org/10.1073/pnas.090091297.
31. Davidson, L., Muniz, L., and West, S. (2014). 3′ end formation of pre-mRNA and phosphorylation of Ser2 on the RNA polymerase II CTD are reciprocally coupled in human cells. Genes Dev. *28*, 342–356. https://doi.org/10.1101/gad.231274.113.
32. Zaborowska, J., Egloff, S., and Murphy, S. (2016). The pol II CTD: new twists in the tail. Nat. Struct. Mol. Biol. *23*, 771–777. https://doi.org/10.1038/nsmb.3285.

33. Shao, W., and Zeitlinger, J. (2017). Paused RNA polymerase II inhibits new transcriptional initiation. Nat. Genet. *49*, 1045–1051. https://doi.org/10.1038/ng.3867.

34. Fan, Z., Devlin, J.R., Hogg, S.J., Doyle, M.A., Harrison, P.F., Todorovski, I., Cluse, L.A., Knight, D.A., Sandow, J.J., Gregory, G., et al. (2020). CDK13 cooperates with CDK12 to control global RNA polymerase II processivity. Sci. Adv. *6*. https://doi.org/10.1126/sciadv.aaz5041.

35. Chen, F.X., Smith, E.R., and Shilatifard, A. (2018). Born to run: control of transcription elongation by RNA polymerase II. Nat. Rev. Mol. Cell Biol. *19*, 464–478. https://doi.org/10.1038/s41580-018-0010-5.

36. Massaiu, I., Songia, P., Chiesa, M., Valerio, V., Moschetta, D., Alfieri, V., Myasoedova, V.A., Schmid, M., Cassetta, L., Colombo, G.I., et al. (2021). Evaluation of Oxford Nanopore MinION RNA-seq performance for human primary cells. Int. J. Mol. Sci. *22*, 6317. https://doi.org/10.3390/ijms22126317.

37. Uszczynska-Ratajczak, B., Lagarde, J., Frankish, A., Guigó, R., and Johnson, R. (2018). Towards a complete map of the human long non-coding RNA transcriptome. Nat. Rev. Genet. *19*, 535–548. https://doi.org/10.1038/s41576-018-0017-y.

38. Cui, Y., and Denis, C.L. (2003). In vivo evidence that defects in the transcriptional elongation factors RPB2, TFIIS, and SPT5 enhance upstream poly(A) site utilization. Mol. Cell Biol. *23*, 7887–7901. https://doi.org/10.1128/mcb.23.21.7887-7901.2003.

39. Liu, X., Freitas, J., Zheng, D., Oliveira, M.S., Hoque, M., Martins, T., Henriques, T., Tian, B., and Moreira, A. (2017). Transcription elongation rate has a tissue-specific impact on alternative cleavage and polyadenylation in Drosophila melanogaster. RNA *23*, 1807–1816. https://doi.org/10.1261/rna.062661.117.

40. Wen, Y., Lu, X., Ren, J., Privratsky, J.R., Yang, B., Rudemiller, N.P., Zhang, J., Griffiths, R., Jain, M.K., Nedospasov, S.A., et al. (2019). KLF4 in macrophages attenuates TNFα-mediated kidney injury and fibrosis. J. Am. Soc. Nephrol. *30*, 1925–1938. https://doi.org/10.1681/asn.2019020111.

41. Tang, T.T., Lv, L.L., Wang, B., Cao, J.Y., Feng, Y., Li, Z.L., Wu, M., Wang, F.M., Wen, Y., Zhou, L.T., et al. (2019). Employing macrophage-derived microvesicle for kidney-targeted delivery of Dexamethasone: an efficient therapeutic strategy against renal inflammation and fibrosis. Theranostics *9*, 4740–4755. https://doi.org/10.7150/thno.33520.

42. Liu, B.C., Tang, T.T., Lv, L.L., and Lan, H.Y. (2018). Renal tubule injury: a driving force toward chronic kidney disease. Kidney Int. *93*, 568–579. https://doi.org/10.1016/j.kint.2017.09.033.

43. Lv, L.L., Feng, Y., Wen, Y., Wu, W.J., Ni, H.F., Li, Z.L., Zhou, L.T., Wang, B., Zhang, J.D., Crowley, S.D., and Liu, B.C. (2018). Exosomal CCL2 from tubular epithelial cells is critical for albumin-induced tubulointerstitial inflammation. J. Am. Soc. Nephrol. *29*, 919–935. https://doi.org/10.1681/asn.2017050523.

44. Lv, L.L., Tang, P.M.K., Li, C.J., You, Y.K., Li, J., Huang, X.R., Ni, J., Feng, M., Liu, B.C., and Lan, H.Y. (2017). The pattern recognition receptor, Mincle, is essential for maintaining the M1 macrophage phenotype in acute renal inflammation. Kidney Int. *91*, 587–602. https://doi.org/10.1016/j.kint.2016.10.020.

45. Jiang, B., Jiang, J., Kaltheuner, I.H., Iniguez, A.B., Anand, K., Ferguson, F.M., Ficarro, S.B., Seong, B.K.A., Greifenberg, A.K., Dust, S., et al. (2021). Structure-activity relationship study of THZ531 derivatives enables the discovery of BSJ-01-175 as a dual CDK12/13 covalent inhibitor with efficacy in Ewing sarcoma. Eur. J. Med. Chem. *221*, 113481. https://doi.org/10.1016/j.ejmech.2021.113481.

46. Hao, S., Salzo, J., Zhao, H., Hao, M., Darzynkiewicz, Z., and Ferreri, N.R. (2020). MicroRNA-133a-Dependent inhibition of proximal tubule angiotensinogen by renal TNF (Tumor Necrosis Factor). Hypertension *76*, 1744–1752. https://doi.org/10.1161/hypertensionaha.120.15435.

47. Conesa, A., Madrigal, P., Tarazona, S., Gomez-Cabrero, D., Cervera, A., McPherson, A., Szcześniak, M.W., Gaffney, D.J., Elo, L.L., Zhang, X., and Mortazavi, A. (2016). A survey of best practices for RNA-seq data analysis. Genome Biol. *17*, 13. https://doi.org/10.1186/s13059-016-0881-8.

48. Alamancos, G.P., Pagès, A., Trincado, J.L., Bellora, N., and Eyras, E. (2015). Leveraging transcript quantification for fast computation of alternative splicing profiles. RNA *21*, 1521–1531. https://doi.org/10.1261/rna.051557.115.